ADVANCED OPTICAL MATERIALS
www.advopticalmat.de

Tetraphenylpyrazine Based AIE Luminogens: Unique Excited State Decay and Its Application in Deep-Blue Light-Emitting Diodes

Lingxiang Pan, Haozhong Wu, Junkai Liu, Kaiqi Xue, Wenwen Luo, Ping Chen, Zhiming Wang, Anjun Qin,* and Ben Zhong Tang**

Carbazole-modified tetraphenylpyrazine (TPP) derivatives TPP-Cz, TPP-PhCz, TPP-2Cz, and TPP-2PhCz are prepared with different patterns by inserting a π-bridge and adopting two-armed forms to produce aggregation-induced emission (AIE)-type deep-blue emitters for organic light-emitting diode (OLED) applications. Systematic spectral analysis and detailed theoretical calculation of these TPP derivatives reveal their special excited state behaviors. Unlike the traditional AIE unit, which features enhanced emission from solution to aggregate with the nonradiative decay channel blocked, a tenfold increase in the radiative decay rate of these TPP-based AIE luminogens (AIEgens) is observed from the solution to film states. The formation of a stable quinone conformation of the TPP center and its peripheral phenyl group in the excited state is the main reason for this behavior. The distribution changes in the total reorganization energy are further integrated, and a feasible molecular design strategy is proposed for the TPP family. Nondoped OLEDs are fabricated, and the AIEgens exhibit good performance with valuable blue emission ($x + y < 0.3$). The TPP-Cz-based optimized devices exhibit more stable external quantum efficiencies and an ideal roll-off with unchanged Commission Internationale de l'Elcairage (CIE) coordinates of (0.16, 0.11). These findings demonstrate the great potential of TPP with its unique excited state characteristics as a deep-blue AIEgen.

1. Introduction

With the commercial application of organic light-emitting diodes (OLEDs) in displays, research on organic luminescent materials has become a hot topic in both academia and industry.[1–5] To achieve an efficient display device, high photoluminescence (PL) efficiencies in film are essential for organic electroluminescent materials.[6–8] However, many luminescent materials exhibit good fluorescence in a unimolecular state (such as in solution) but become weak emitters when assembled as nanoparticles or fabricated into films (aggregate state) in practical applications. This change in behavior is mainly due to the formation of detrimental species such as excimers and exciplexes in the condensed phases, known as the aggregation-caused quenching (ACQ) effect.[9–11] Various approaches based on chemical, physical, and engineering processes have been adopted to enhance their emission; however, limited success has been achieved because of the natural process of molecular aggregation.[12,13]

A strategy of "aggregation-induced emission" (AIE) that utilizes the molecular aggregation rather than fighting against it to enhance the emission of luminogens was presented by Luo et al. in 2001.[14–17] Usually, AIE luminogens (AIEgens) are nonemissive in dilute solution but remarkably emissive upon the formation of aggregates or fabrication into a solid film, which is beneficial for constructing high-efficiency nondoped OLEDs.[18–29] To date, numerous AIE materials with good performance for red, yellow, green, and blue emission have been developed.[22,23,25,30–33] However, outstanding blue AIE materials, especially deep-blue ones are rare.[32] Tetraphenylethylene[34] (TPE) and 1,1,2,3,4,5-hexaphenyl-silole[35] (HPS) are the most studied AIE systems, and many high-efficiency AIEgens

L. Pan, H. Wu, J. Liu, W. Luo, Prof. Z. Wang, Prof. A. Qin, Prof. B. Z. Tang
State Key Laboratory of Luminescent Materials and Devices
Center for Aggregation-Induced Emission
South China University of Technology
Guangzhou 510640, China
E-mail: wangzhiming@scut.edu.cn; msqinaj@scut.edu.cn; tangbenz@ust.hk

The ORCID identification number(s) for the author(s) of this article can be found under https://doi.org/10.1002/adom.201801673.

DOI: 10.1002/adom.201801673

K. Xue, Prof. P. Chen
State Key Laboratory on Integrated Optoelectronics
Jilin University
Changchun 130012, China

Prof. B. Z. Tang
Department of Chemistry
Hong Kong Branch of Chinese National Engineering Research Center for Tissue Restoration and Reconstruction
Institute for Advanced Study
and Department of Chemical and Biological Engineering
The Hong Kong University of Science and Technology
Clear Water Bay, Kowloon, Hong Kong 999077, China

based on their skeleton structures for OLEDs have been developed. Nevertheless, both TPE and HPS emit at a relative long wavelength with broad emission band, and the performance of their derivatives is insufficient for preparing deep-blue AIEgens. Although tuning the bonding pattern or twisting dihedral angles could enable control of their intramolecular conjugation effect to shift their emission to a bluer region, it is difficult to simultaneously achieve higher efficiencies.[36]

Tetraphenylpyrazine (TPP), a new AIE-active-core, was developed by Chen et al. in 2015 with the advantages of facile preparation, easy modification, and excellent thermal and photo stability.[37–39] Moreover, the emission of the naked TPP unit occurs at ≈390 nm with a narrow full width at half maximum (FWHM), which is beneficial for constructing deep-blue AIE emitters for OLED applications. In our previous work, triphenylamine (TPA)-modified TPP derivatives were prepared and exhibited good OLED performance; however, their emission occurred in the sky-blue region, which is unfavorable for the fabrication of efficient deep-blue OLEDs.[38] The D–A interaction between TPA and the TPP moiety is too strong, leading to a redder emission peak. Moreover, the increased rotational freedom of the TPA unit in the excited state can widen the emission spectra, demolishing the purity of the blue light emission. Here, we employ the carbazole (Cz) group instead of the TPA unit, which would result in a weaker electron-donating ability and restrict rotation via a locked single bond, and TPP-Cz was primitively prepared. To obtain a better understanding of the structure–property relationships in TPP-based AIEgens, π-bridge and double-armed patterns were introduced, and TPP-PhCz, TPP-2Cz, and TPP-2PhCz were obtained, as illustrated in **Figure 1**.

All these TPP-based compounds exhibited obvious AIE activities. Systemic spectra characterization and theoretical calculation simulations in ground and excited states from unimolecular states to aggregate ones help to clarify the changing trend between their radiative/nonradiative decay processes with the different chemical coupling patterns. Interestingly, the unique excited state characteristics of TPP-based AIEgens are found, which could serve as a validated molecular design strategy for the construction of high efficiency blue emitters. Nondoped OLEDs were fabricated with expected deep-blue emission, and the TPP-Cz based device was optimized with better performance and lower current efficiency roll-off under high brightness. All these results demonstrate the potential of TPP as a deep-blue emission AIEgen owing to its unique excited state characteristics.

2. Results and Discussion

2.1. Synthesis and Crystal Analysis

The four target carbazole-functionalized TPP derivatives, TPP-Cz, TPP-2Cz, TPP-PhCz, and TPP-2PhCz, were synthesized according to the synthetic routes described in Figure 1 (the detailed synthetic procedures and characterization data are provided in the Supporting Information). The intermediate of TPP-Br was prepared according to the methods previously reported in the literatures,[37–40] and the Ullman coupling reaction was used for the preparation of TPP-Cz in a yield of 62%. To demonstrate the flexibility of the synthetic method for TPP-based compounds, TPP-2Cz was prepared via the condensation reaction using ortho-dione and ortho-diamine derivatives. For TPP-PhCz and TPP-2PhCz, the Suzuki coupling reaction from TPP-Br or TPP-2Br with boric-carbazole catalyzed by $Pd(PPh_3)_4$ was the best choice. All the structures were spectroscopically characterized using proton and carbon nuclear magnetic resonance (NMR) spectroscopy and high-resolution mass spectroscopy (HRMS), together with X-ray crystallography, and satisfactory data were obtained (**Figure 2** and Figures S1–S20, Supporting Information).

Single crystals were grown from methanol/dichloromethane or methanol/tetrahydrofuran (THF) mixtures, and detailed analyses of the resulting X-ray diffraction (XRD) data are shown in Figure 2 and X-ray crystallography in the Supporting Information. Similar to the TPE derivatives in single-crystal form, the four peripheral phenyl groups in TPP underwent nonplanar but propeller-shaped conformations with twisted angles in the range of 30° to 57° around the pyrazine center, and the coupled carbazole group was highly twisted with the neighboring phenyl plane. In addition, the central pyrazine ring was not a rigid plane, as imagined, but a warped one, and their twist angles could reach as large as 12°, suggesting that the conjugation of these TPP derivatives would be limited to some degree by the pyrazine center bridge. Moreover, the insertion of a phenyl group as a π-bridge in TPP-Cz→TPP-PhCz or TPP-2Cz→TPP-2PhCz interrupted the conjugation between TPP and the carbazole group because of the increase of the twist angle. For example, the angle between the phenyl plane and carbazole plane changed from 55.16° in TPP-Cz to 70.28° in TPP-PhCz, which would affect their spectra in solution or aggregates. Overall, all these factors appear to indicate that it may be an ideal candidate to construct blue emitters using these TPP-based materials.

Observing the molecular packing modes, the multiple intermolecular C—H···π hydrogen bonds with distances in the range of 2.71–3.49 Å between the adjacent molecules were disclosed, as marked in Figure 2, and these interactions rigidify the molecular conformation and lock the molecular rotation in the crystal lattice, which is beneficial in reducing the nonradiative deactivation of excitons and enabling them to emit intensely in aggregate states. Consequently, these TPP-based materials might have AIE or AEE characteristics, similar to those of a TPE derivative.

However, the ratio of free space volume was increased when the π-bridge (TPP-Cz→TPP-PhCz) or the double-arm substituted form (TPP-Cz→TPP-2Cz) was introduced. Even in TPP-2PhCz, the solvent molecule was observed in the crystal lattice. In fact, this unoccupied space would increase the probability for molecules to vibrate and rotate when they obtained energy, leading to an increase in the nonradiative deactivation. Additionally, it is worth noting that the warped pyrazine center almost had no interactions with its surrounding structures, indicating that the motion of the pyrazine ring could not be restricted in the aggregate state. Correspondingly, the AIE behavior would become very unpredictable because aforementioned factors might go against the AIE behaviors of these TPP-based derivatives; however, further verification is required.

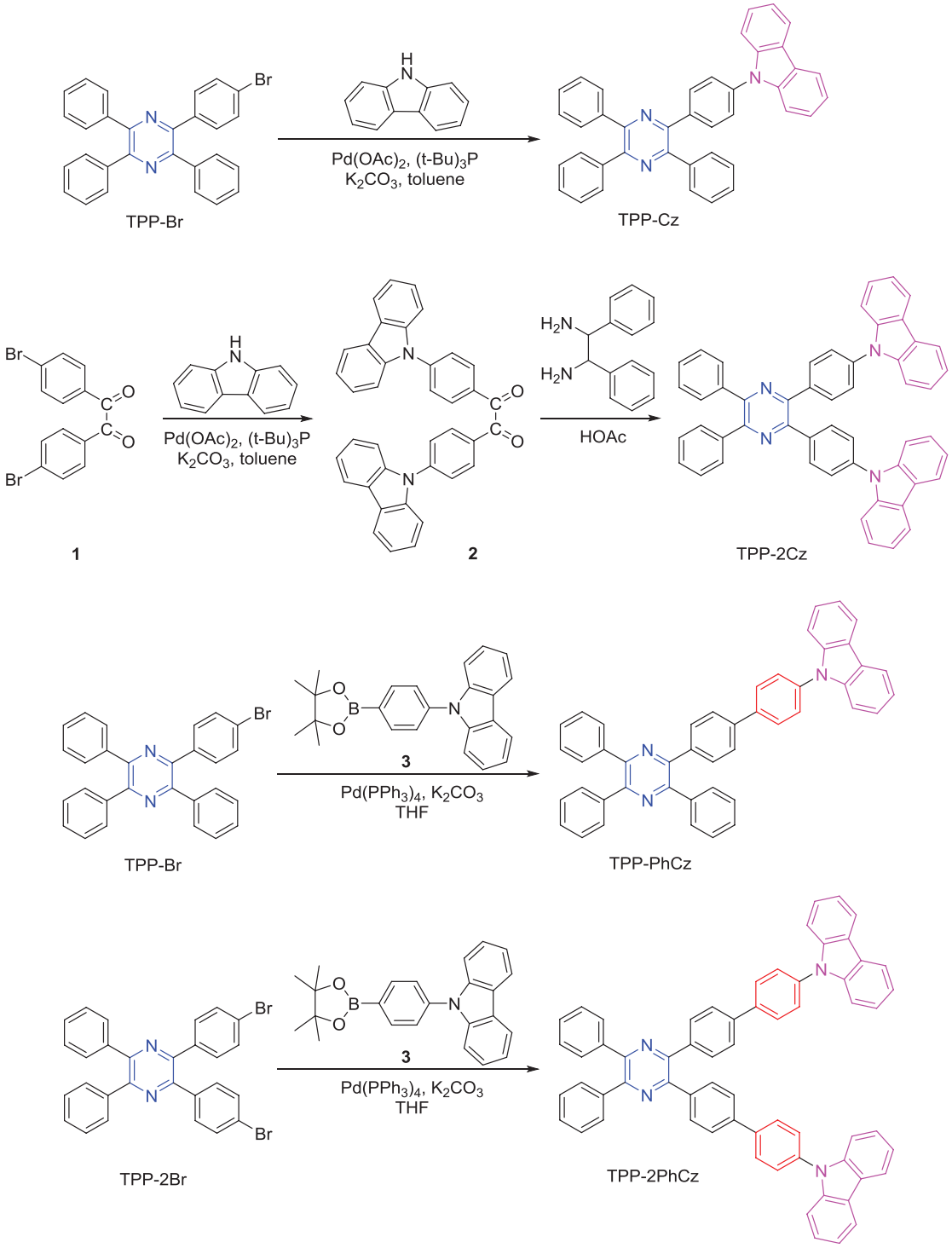

Figure 1. Synthetic routes toward carbazole-functionalized TPP derivatives TPP-Cz, TPP-2Cz, TPP-PhCz, and TPP-2PhCz.

2.2. Thermal Stability

Generally, good thermal stability of the emitters is essential for the process of vacuum deposition and for the operating stability of light-emitting devices. The thermal stability of TPP-Cz, TPP-2Cz, TPP-PhCz, and TPP-2PhCz were investigated using thermogravimetric analysis (TGA) at a heating rate of 20 °C min^{-1} under nitrogen condition (Figure S21, Supporting Information). The TPP derivatives exhibit good thermal stability with temperatures of 5% weight loss (T_d) as high as 335, 424, 411, and 529 °C for TPP-Cz, TPP-2Cz, TPP-PhCz, and TPP-2PhCz, respectively. Moreover, no obvious glass transition

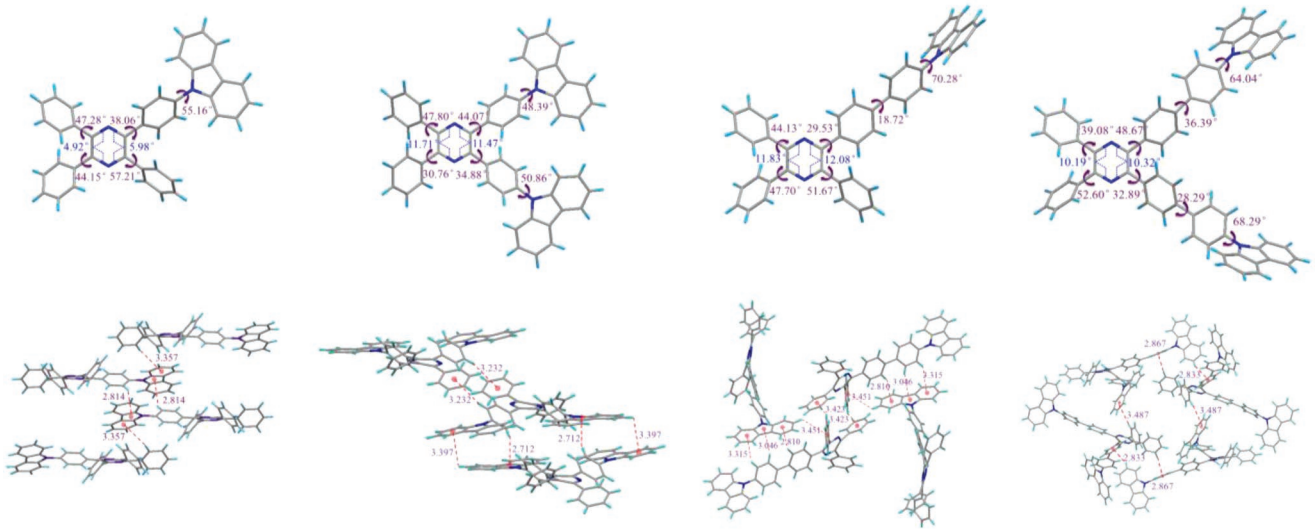

Figure 2. Crystal structures, torsion angles and CH···π hydrogen bonds formed between the adjacent molecules of TPP-Cz, TPP-2Cz, TPP-PhCz, and TPP-2PhCz.

temperature (T_g) was observed in their differential scanning calorimetry (DSC) measurements, suggesting their good morphological stability.

2.3. Photophysical Properties

The TPP-based derivatives exhibit good solubility in common organic solvents but are insoluble in water. As shown in **Figure 3**A, they exhibited almost the same absorption spectra profiles with two main absorption peaks in THF solution: the peak at ≈292 nm corresponds to the typical absorption of the carbazole group, and the peak at 343 nm with a stronger and broader band should be the maximum absorption (λ_{abs}) wavelength derived from the π–π^* transition of these TPP derivatives.

The slight change occurring from TPP-Cz to TPP-PhCz or from TPP-2Cz to TPP-2PhCz is thought to originate from the synergistic effect between the larger π-system and the more twisted angle when the phenyl group was inserted, wherein the former usually results in a bathochromic shift of the absorption spectrum because of the extension of the electron delocalization, and the latter often induces a blue-shift of the spectrum because of the decrease in the conjugation. Moreover, compared with monosubstituted derivatives, the small changes in disubstituted ones can be attributed to their similar transition absorption from the carbazole group to the TPP center, which will be confirmed in the subsequent theoretical analysis.

Similar negligible changes of the fluorescence spectra both in solution and films were observed for these TPP derivatives. In THF, they exhibited blue emission with peaks at 436–447 nm and low quantum yields (Φ_s) of ≈1–2% (**Table 1**; Figure S22, Supporting Information); however, in films, their emission was enhanced with higher Φ_s of 21.1%, 20.5%, 23.6%, and 14.8% for TPP-Cz, TPP-2Cz, TPP-PhCz, and TPP-2PhCz, respectively, demonstrating their AIE feature. More importantly, no obvious

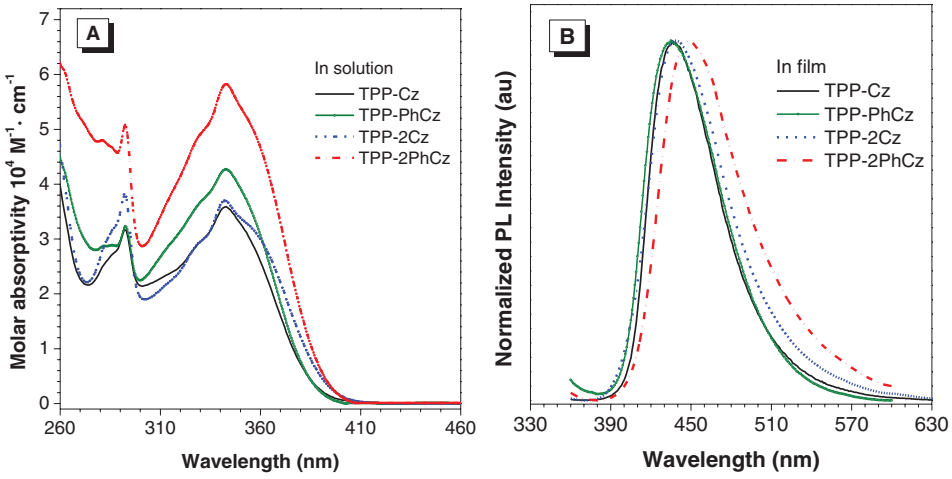

Figure 3. A) UV spectra in THF solutions (10×10^{-6} M) and B) PL spectra in solid films of TPP-Cz, TPP-PhCz, TPP-2Cz, and TPP-2PhCz.

Table 1. The photophysical data of TPP-Cz, TPP-2Cz, TPP-PhCz, and TPP-2PhCz.

Compound	λ_{abs} [a] [nm]	λ_{em} [b] [nm]				Φ_F [c] [%]		τ [d] [ns]		K_r [e] [10^7 s^{-1})]		K_{nr} [f] [10^7 s^{-1}]	
		Soln	FWHM	Film	FWHM	Soln	Film	Soln	Film	Soln	Film	Soln	Film
TPP-Cz	292, 343	440	69	436	60	0.8	21.1	0.57	1.05	1.40	20.10	174.04	75.14
TPP-2Cz	292, 343	447	71	438	67	1.5	20.5	0.57	1.05	2.63	19.52	172.81	75.71
TPP-PhCz	292, 343	436	75	435	65	0.9	23.6	0.59	0.78	1.51	30.26	167.97	97.95
TPP-2PhCz	292, 343	444	76	449	71	1.5	14.8	0.65	0.78	2.31	18.97	151.54	109.23

[a]Absorption peaks, concentration: 10×10^{-6} M; [b]Maximum emission wavelength, Soln: THF solution, Film: droplet film, FWHM: full width at half maximum; [c]absolute fluorescence quantum efficiency; [d]fluorescence lifetime; [e]$K_r = \Phi_F/\tau$; [f]$K_{nr} = (1 - \Phi_F)/\tau$.

red-shift was observed in their maximum fluorescence peaks, and all of their emissions were located in the deep-blue emission region with FWHMs as narrow as ≈70 nm in the films, implying their good color purity.

To further verify the AIE feature, the emission behaviors of TPP derivatives in THF/water mixtures with different water fractions (f_w) were studied (**Figure 4** and Figure S23, Supporting Information). As depicted in Figure 4A, TPP-Cz exhibited faint emission in diluted THF solution, and its intensity increased slightly when the water fraction was less than 70%. Once $f_w > 70\%$, swift enhancement of the emission intensity was observed because of the formation of aggregates, which is a typical AIE phenomenon. Detailed investigation of the spectrum showed that a red-shifted trend was first observed at low f_w because of the occurrence of the charge transfer when the solvent polarity increased with the addition of high polar water. Afterward, the emission peaks blue shifted at higher f_w due to the decrease of solvating ability of the mixture solvent and the emission intensity becomes stronger because of the restriction of intramolecular motion (RIM)[41] at the same time. Similar AIE behaviors of TPP-2Cz, TPP-PhCz, and TPP-2PhCz were observed (Figure 4B).

To better understand the photophysical properties of these new AIEgens, the rates of radiative decay (K_r) and nonradiative decay (K_{nr}) in solution and film states were calculated from their Φ_s and lifetime (τ), and the results are presented in Table 1. The lifetime was estimated from the time-resolved fluorescence spectra (Figure S24, Supporting Information). For most AIEgens, the enhancement of their PL intensities from solution to solid state is usually derived from the synergistic effect of the increase of K_r and the decrease of K_{nr}, with the latter typically playing a major role in the stator–rotor model of the RIM mechanism, such as TPE or siloles. However, as shown in Table 1, the K_r in the film states of these TPP derivatives increased dramatically by ten times compared with the values in solution states, while, their K_{nr} values only slightly decreased, which contrasts greatly with the behavior of traditional AIEgens, implying their unique excited state in the emission process.

In addition, we observed that the monocarbazole- and monophenylcarbazole substituted TPPs (TPP-Cz and TPP-PhCz) and di-carbazole and di-phenylcarbazole-substitued ones (TPP-2Cz and TPP-2PhCz) had almost the same fluorescence lifetimes in solution and film states, indicating that their emission might originate from the similar species. In other words, the performances of the disubstituted TPPs appeared to originate from the superposition of monosubstituted ones.

2.4. Luminescence Process

To obtain an in-depth understanding of the emission process of these TPP-based derivatives at a molecular level, density

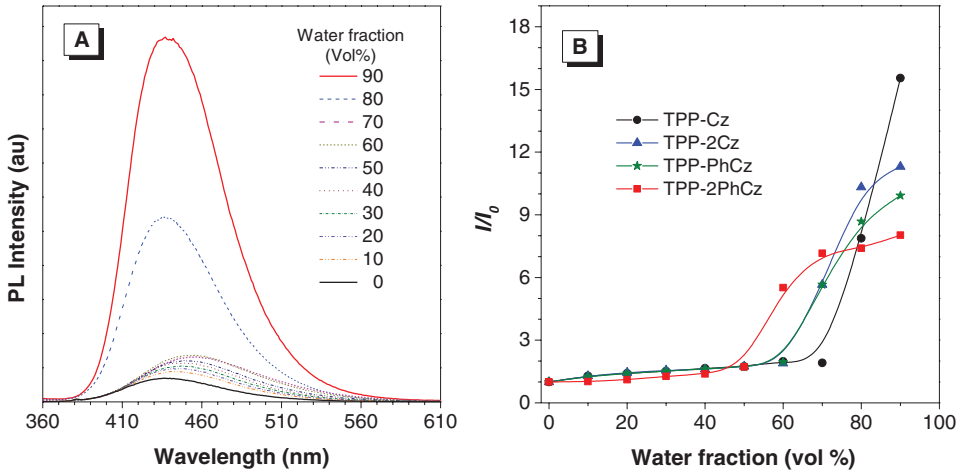

Figure 4. A) PL spectra of TPP-Cz in THF/water mixtures with different water fractions; excitation wavelength: 343 nm; concentration: 10×10^{-6} M. B) Plot of (I/I_0) value in THF/water mixtures of TPP-Cz, TPP-2Cz, TPP-PhCz, and TPP-2PhCz; I_0 refers to the original emission intensity in THF.

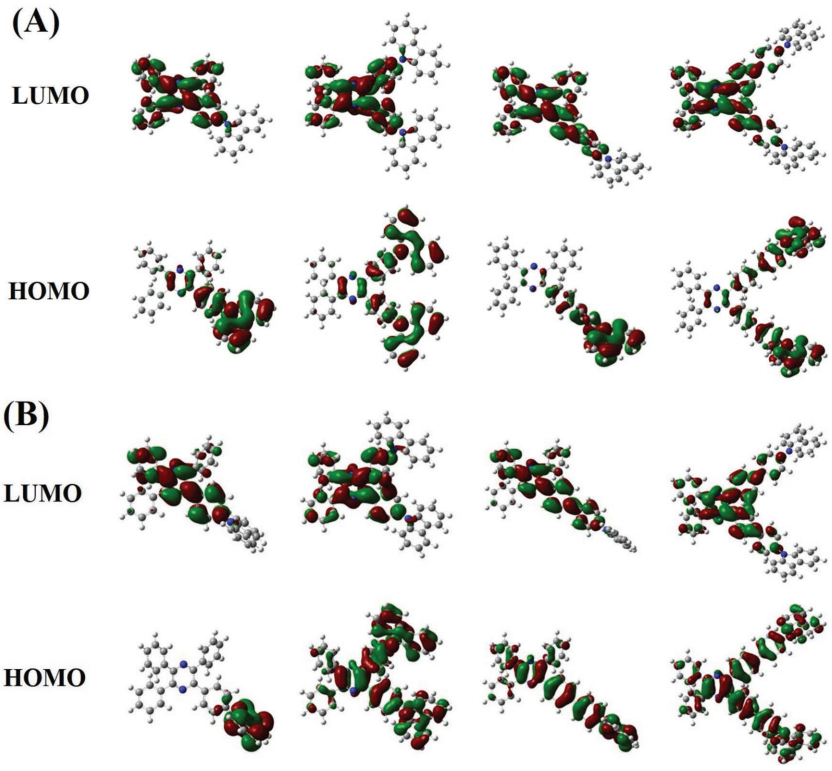

Figure 5. HOMO/LUMO distributions of TPP-Cz, TPP-2Cz, TPP-PhCz, and TPP-2PhCz: A) in ground states and B) in excited states.

functional theory (DFT) and time-dependent density functional theory (TD-DFT) calculations using the B3LYP/6-31G(d) method were carried out, from which the detailed information on the molecular conformations and the highest occupied molecular orbitals (HOMOs)/the lowest unoccupied molecular orbitals (LUMOs) distributions in ground and excited states were obtained. As illustrated in **Figure 5**, the optimized geometries of the AIEgens in the gas phase adopt obvious twisted conformations, which is consistent with that in their crystal state.

In ground state, the HOMOs of these AIEgens are primarily dominated by the orbitals from the carbazole and π-bridge phenyl groups, whereas the LUMOs are mainly located at the TPP core. These findings are consistent with their similar absorption spectra and maximum absorption wavelength. For the excited state, their radiative transition of $S_1 \rightarrow S_0$ consists mainly of the form of LUMO→HOMO in these TPP derivatives. In TPP-Cz and TPP-PhCz, the electron clouds spread mainly along the axis direction of the substituents from the pyrazine to the carbazole units, and little lied on the abaxial phenyl group, indicating that the groups along the axis direction dominated the radiation transition process.

The changes of the bond length and dihedral angles (Tables S1 and S2, Supporting Information) in TPP-Cz and TPP-PhCz from the ground to excited state are shown in **Figure 6**. The bond lengths of N1—C2, N4—C5, C3—C8, and C6—C10 are shortened (the trend of forming a double bond), the bond lengths of C2—C3, C3—N4, C5—C6, and C6—N1 are elongated (the trend of forming a single bond), and the bond lengths of C2—C7 and C5—C9 changed little. In addition, the dihedral angles of α_2, α_4, and β_1 became smaller, demonstrating a planarization trend of the whole molecule along the axial direction of the substituents. All these changes are the result of the formation of the quinone structure in the excited state, which is consistent with the HOMO and LUMO distributions shown in Figure 5B. Moreover, the stable quinone conformation of the pyrazine ring in the excited state greatly contributes to the formation of the axis luminescence process.

Assuming that these unique changes in the excited state can be attributed to an extramalization, the emission behavior of monosubstituted TPP derivatives was only affected by the substituted groups along the axis, and the process can be described simply as "line-type emission" (LE). Accordingly, the disubstituted TPP derivatives of TPP-2Cz and TPP-2PhCz feature "X-shaped emission" (XE). This assumption could be supported by following issues: 1) the distributions of the HOMO and LUMO of TPP-2Cz and TPP-2PhCz appear to correspond to the crossing axis view of TPP-Cz and TPP-PhCz. In addition, similar absorption and emission spectra, and even their fluorescence lifetime, were observed for the mono- and di-substituted TPP derivatives, indicating their identical or similar emission species; 2) as proven by theory simulation (the data were summarized in Table S1, Supporting Information); all the dihedral angles of α_1, α_2, α_3, α_4, β_1, and β_2 decreased significantly, suggestive of better planarity of these molecules and further confirming our speculation of the luminescence mechanism; 3) the efficiency of the molecules in solution states increased. Although the absorption of four TPP derivatives is similar, the quantum yield of TPP-2Cz is almost two times higher than that of TPP-Cz. Meanwhile, similar result was found for TPP-2PhCz and TPP-PhCz (Table 1). This phenomenon could be ascribed to the independent emission from the axes.

Additionally, compared with the structures of these AIEgens in the crystalline states, their dihedral angles of N1—C2—C3—N4 and N4—C5—C6—N1 are much larger in the gas state as shown by the theoretical calculation. Taking TPP-Cz as an example, the dihedral angles of N1—C2—C3—N4 and N4—C5—C6—N1 in excited state are 19.26° and 21.45°, respectively, whereas in the crystalline state, these values are only 4.92° and 5.78°, respectively. The decrease of the dihedral angles in the pyrazine ring suggests that the AIEgens possess a more planar conformation in the real world which will explain why the K_r values of these TPP derivatives in film states are approximately ten times larger than those in solution.

2.5. Reorganization Energy Calculation

As mentioned above, no significant decrease of the nonradiative decay rate of these TPP derivatives was observed from the solution to aggregate state, which differs from the behavior of

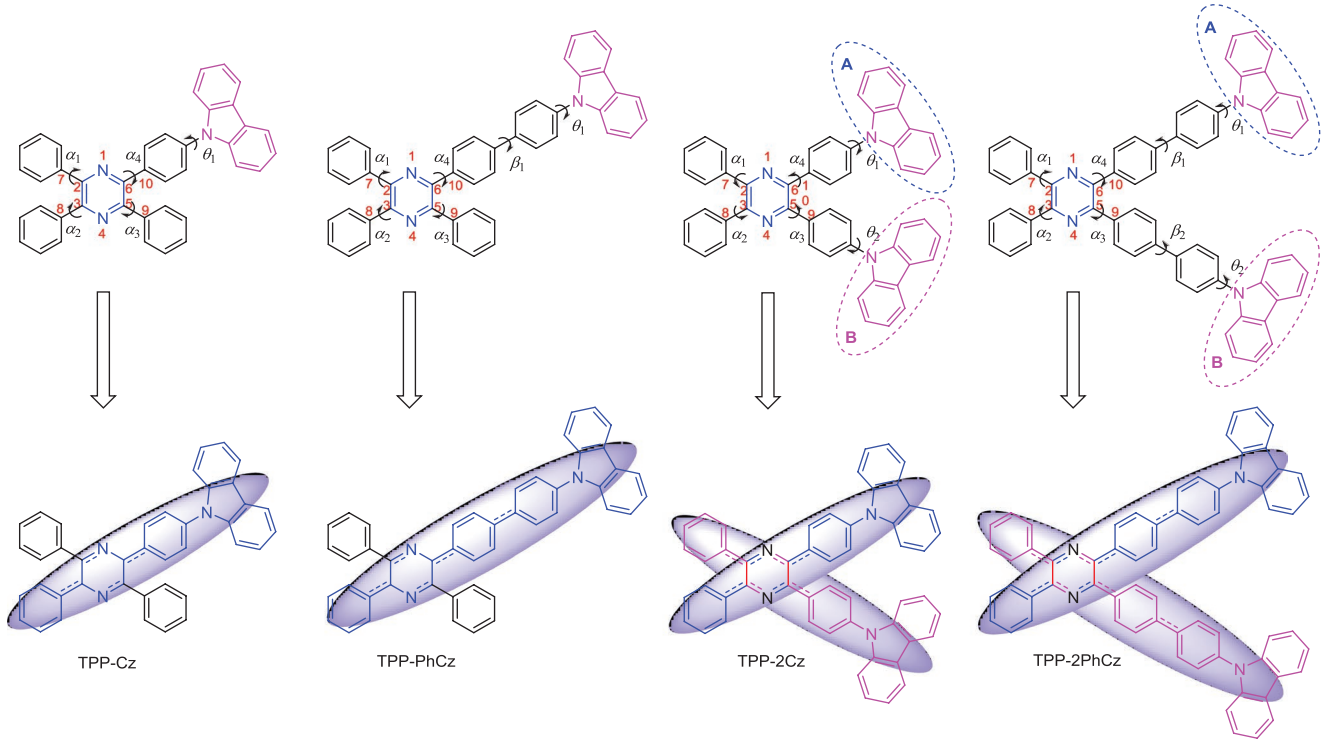

Figure 6. Top: The marks of the atoms and the twist angles of TPP-Cz, TPP-PhCz, TPP-2Cz, and TPP-2PhCz; bottom: the "line-typed" and "X-shaped" luminescence mechanism of these AIEgens.

traditional AIEgens that their enhanced emission is ascribed to the decrease of nonradiative decay, whereas, the radiative decay remains almost no change. Hence, elaborating the cause of this differing behavior is critical for TPP-based AIEgens. We thus investigated the reorganization energy of these AIEgen both in gas phase state and crystalline phase state (**Figure 7** and Figures S25 and S26, Supporting Information). It is worth noting that this investigation was generally used for the discussion of the excited-state relaxation dynamics and nonradiative decay process of traditional AIEgens.[42]

Generally, there are two parts that contribute to the total reorganization energy: the low-frequency motion modes (<1000 cm^{-1}) and the high-frequency motion modes (>1000 cm^{-1}). The former mainly originates from the adjustment of the dihedral angle by the rotation of the substituents, which could be blocked by intermolecular packing, and most of the AIEgens undergo this process. The latter represents the vibrations of the intramolecular bonds, which are generally affected by chemical structures and show little dependence on the stacking patterns.

The calculated reorganization energy of these TPP derivatives is listed in **Table 2**. As we can find that a large proportion of the high-frequency motion modes, which are mostly related to the bond-stretching occured both in the gas and solid states, this behavior remarkably differs from that of the traditional AIEgens, whose low-frequency rotation modes play key roles.[43,44]

Taking TPP-PhCz as an example, its total reorganization energy is deduced to be 2159.33 cm^{-1}, with the low-frequency rotation mode accounting for 43% (923.48 cm^{-1}) and the high-frequency bond-stretching one accounting for 51% (1094.69 cm^{-1}) in the gas state (Table 2). While, in the solid state, the total reorganization energy decreases to 1901.61 cm^{-1}. However, only slight abatement of the high-frequency bond-stretching modes with a reorganization energy of 954.21 cm^{-1} (50% of the total one) was observed. Similarly, the low-frequency motion mode in TPP-Cz also clearly decreased from 2122.25 cm^{-1} in the gas state to 385.05 cm^{-1} in the solid state, indicating that the rotation modes were restricted efficiently, while, the proportion of the high-frequency motion modes remained dominant in the solid state. This result suggests that the continuous presence of large numbers of nonradiative transition channels could not be blocked by the molecular packing, which well explains why TPP-based AIEgens possess relatively weak emission compared with that of TPE derivatives.

Furthermore, the detailed motions of these TPP derivatives were studied and the data are summarized in Tables S3–S9 in the Supporting Information, which indicate that the reorganization energy of the bond-stretching modes (the high-frequency motion mode) mainly originated from the pyrazine ring. Again, taking TPP-PhCz as an example, as shown in Table 2 and Tables S5–S6 in the Supporting Information, the reorganization energy of the bond-stretching modes related to the pyrazine ring (N1—C4, N1—C7, N2—C5, N2—C6, C4—C5, C6—C7, C4—C8, C5—C19, C6—C30, and C7—C70, marks show the optimized structure of TPP-PhCz in Table S5 in the Supporting Information reached 570.03 cm^{-1} in the gas state, which made up 52.07% of the total one (1094.69 cm^{-1}). In the solid state, the pyrazine-ring-related reorganization energy of the bond-stretching modes came to 435.01 cm^{-1} (45.59% of

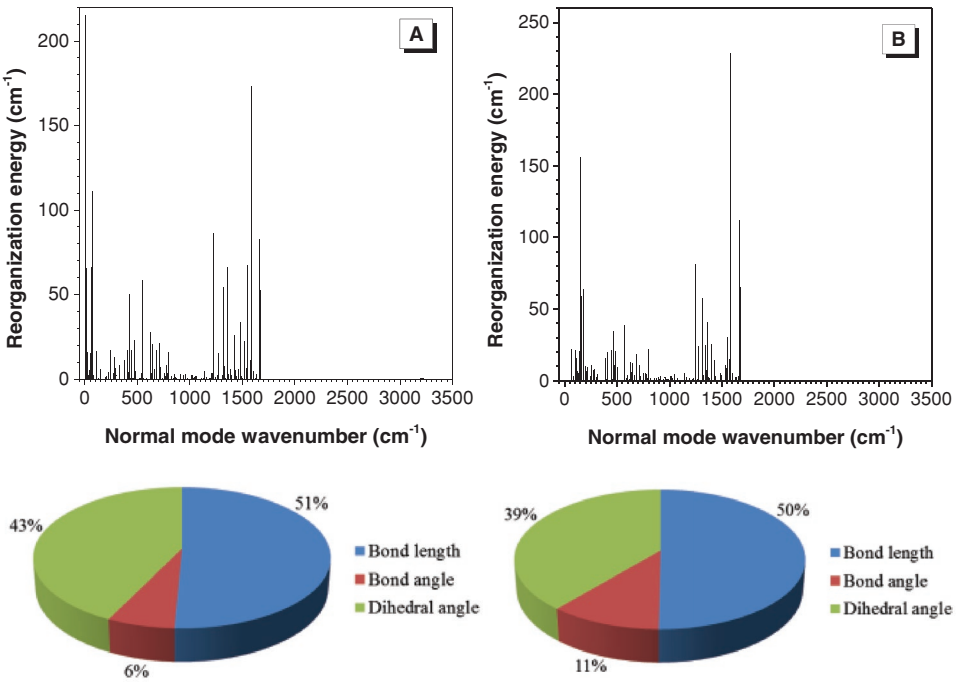

Figure 7. Presentation of the calculated reorganization energy versus the normal mode wave numbers and the contribution to the total reorganization energy from the bond length, the bond angle, and the dihedral angle of TPP-PhCz in gas state (A) and solid state (B). The changes of the bond length and the dihedral angle mainly refer to stretching and rotational motions, respectively.

the total one). Moreover, the highest three values of the reorganization energy from the bond-stretching motion modes of TPP-PhCz both in the gas (C6—C30, C6—C7, and N2—C6) and solid (N2—C6, C6—C30, and N1—C4) states all originated from the pyrazine ring. Therefore, it is apparent that the limitation of the high-frequency motion modes of the pyrazine ring in TPP-based AIEgens is critical to improve the emission efficiency in both gas and solid states.

From this viewpoint, tuning of the chemical structure of the TPP derivatives to decrease the high-frequency motion modes of the pyrazine ring and increase the conjugation or rigidity of the pyrazine ring appeared to be a good strategy. From TPP-Cz to TPP-PhCz, the contribution of the reorganization energy from the high-frequency motions (including vibration of the bond angle and bond length) decreased from 1534.64 cm^{-1} (1200.29 + 334.35 cm^{-1}) for TPP-Cz to 1235.85 cm^{-1} (1094.69 + 141.16 cm^{-1}) for TPP-PhCz in the gas states, and this type of trend (more bonds, less energy) was also observed in the solid states (1178.52 to 1162.46 cm^{-1}). From TPP-Cz to TPP-2Cz, a similar situation was observed.

However, the disubstituted molecules could generate free volume during their packing in the aggregate state due to their loose packing, which usually leads to an increase of the rotation modes and results in a reduced efficiency in the solid state. For instance, the reorganization energy from the low-frequency rotation mode increased from 385.05 cm^{-1} for TPP-Cz to 693.03 cm^{-1} for TPP-2Cz. Compared with TPP-Cz, TPP-PhCz possesses from loose packing with 739.15 cm^{-1} of the reorganization energy from the low-frequency rotation mode. For TPP-2PhCz, the reorganization energy became difficult to

Table 2. Reorganization energy of TPP-Cz, TPP-2Cz, TPP-PhCz, TPP-2PhCz, and their distributions.

Compound	Gas state [a] [reorganization energy: cm^{-1}, distributions: %]					Solid state[b] [reorganization energy: cm^{-1}, distributions: %]				
	$\tilde{V}_{Total}$ [c]	$\tilde{V}_{Rotation}$ [d]	$\tilde{V}_{Angle}$ [e]	$\tilde{V}_{Length}$ [f]		$\tilde{V}_{Total}$ [c]	$\tilde{V}_{Rotation}$ [d]	$\tilde{V}_{Angle}$ [e]	$\tilde{V}_{Length}$ [f]	
				$\tilde{V}_{BS}$ [g]	$\tilde{V}_{core}$ [h]				$\tilde{V}_{BS}$ [g]	$\tilde{V}_{core}$ [h]
TPP-Cz	3656.89	2122.25 (58%)	334.35 (9%)	1200.29 (33%)	601.06 (50%)	1563.57	385.05 (25%)	239.64 (15%)	938.88 (60%)	619.35 (66%)
TPP-2Cz	1920.41	892.33 (46%)	131.87 (7%)	896.21 (47%)	607.98 (68%)	1744.88	693.03 (40%)	139.26 (8%)	912.59 (52%)	631.38 (69%)
TPP-PhCz	2159.33	923.48 (43%)	141.16 (6%)	1094.69 (51%)	570.03 (52%)	1901.61	739.15 (39%)	208.25 (11%)	954.21 (50%)	435.01 (45%)
TPP-2PhCz	2497.45	1180.14 (48%)	110.96 (4%)	1206.35 (48%)	694.42 (57%)	–	–	–	–	

[a]Unimolecular state in gas; [b]Solid state in crystal, the reorganization energy of TPP-2PhCz was not obtained because of the solvent molecule in crystal lattice; [c]The total reorganization energy ($\tilde{V}_{Total}$); [d]The contributions from the dihedral angle (rotation) ($\tilde{V}_{Rotation}$); [e]The contributions from the bond angle ($\tilde{V}_{Angle}$); [f]The contributions from the bond length ($\tilde{V}_{Length}$); [g]The total reorganization energy from bond length (stretching) ($\tilde{V}_{BS}$); [h]The bond stretching reorganization energy related to the pyrazine core ($\tilde{V}_{core}$) and the ratio in parentheses is $\tilde{V}_{core}$ divided by $\tilde{V}_{BS}$.

Table 3. Values of OLEDs based on TPP-Cz, TPP-2Cz, TPP-PhCz, and TPP-2PhCz. Abbreviations: λ_{EL} = EL maximum; V_{on} = turn-on voltage at 1 cd m^{-2}; L_{max} = maximum luminance; $\eta_{c,max}$ = maximum current efficiency; $\eta_{ext,max}$ = maximum external quantum efficiency; $\eta_{P,max}$ = maximum power efficiency; $\eta_{C,100}$ and $\eta_{C,1000}$ = current efficiency at 100 and 1000 cd m^{-2} luminance; RO = Current efficiency roll-off from maximum value to that at 1000 cd m^{-2}; CIE [*x*,*y*] = Commission International de l'Eclairage coordinates.

Device	λ_{EL} [nm]	V_{on} [V]	L_{max} [cd m^{-2}]	$\eta_{c,max}$ [cd A^{-1}]	$\eta_{ext,max}$ [%]	$\eta_{P,max}$ [lm W^{-1}]	$\eta_{C,100}$ [cd A^{-1}]	$\eta_{C,1000}$ [cd A^{-1}]	RO [%]	CIE [*x*, *y*]
I-1	472	4.0	2026	0.95	0.51	0.65	0.82	0.71	25.3	0.19, 0.23
I-2	452	3.8	2106	1.01	0.77	0.63	1.00	0.86	14.9	0.15, 0.11
I-3	448	3.8	1931	0.60	0.52	0.50	0.53	0.46	23.3	0.16, 0.12
I-4	464	4.2	2862	0.82	0.70	0.62	0.73	0.76	7.3	0.15, 0.12
II-1	436	3.5	2433	0.98	1.14	0.74	0.97	0.58	40.8	0.15, 0.10
III-1	436	3.7	2608	1.21	1.25	0.93	1.17	1.05	13.2	0.16, 0.11
IV-1	436	3.9	1633	1.09	1.49	0.69	1.04	0.96	11.9	0.16, 0.11
V-1	436	3.6	2264	1.20	1.49	0.91	1.20	1.16	3.3	0.16, 0.11

estimate because of the insertion of solvent molecules in the crystal.

In contrast with TPP-Cz, TPP-2Cz and TPP-PhCz showed a positive effect of expanding the conjugation but suffered from energy consumption owing to the increase of the rotation motions. Hence, their Φ_s in solid states changed little under the synergistic effect. In TPP-2PhC, the negative effect occupied the dominant position in the solid state, and its Φ was only 14.8%.

As previously mentioned, the pyrazine ring cores in these TPP-based AIEgens play an important role in their nonradiative decay process because of its warped structure distortion, and it is not easy to restrict this process. Herein, to prepare high-efficiency TPP-based emitters, it appears to be a more effective strategy to increase K_r by expanding larger conjugation than by tuning K_{nr} through inserting some restricted intramolecular rotation (RIR)-type substitutes with more free space.

2.6. Electroluminescence

Because of the deep-blue emission with smaller FWHM of these TPP-based AIEgens in film state, their nondoped electroluminescence (EL) devices were fabricated. The energy levels of these AIEgens were first estimated using cyclic voltammetry (CV) and the optical bandgap from their absorption spectra. As shown in Figure S27 in the Supporting Information, their redox potential in the positive direction is located almost at the same level. Thus, the values of the HOMOs were estimated from the onset oxidation potential using the following equation: $E_{HOMO} = -(E_{onset} - E_{Fc/Fc^+} + 4.8)$ eV, with $E_{Fc/Fc^+} = 0.40$ eV as tested (Figure S27, Supporting Information) and those of the LUMOs were also calculated using the following equation: $E_{HOMO} = E_{LUMO} + E_g$, with $E_g = 1240/\lambda_{onset}$ (the onset was calculated based on the onset of absorption). As shown in Table S10 in the Supporting Information, the HOMO values of TPP-Cz, TPP-2Cz, TPP-PhCz, and TPP-2PhCz were estimated to be −5.26, −5.27, −5.26, and −5.28 eV, respectively. Their corresponding LUMO energy levels were deduced to be −2.06, −2.12, −2.05, and −2.12 eV, respectively. It is worth noting that there was no significant difference between them.

Afterward, the devices with configurations of ITO/MoO_3 (10 nm)/1,1-bis[4-[*N*,*N*-di(p-tolyl)amino]phenyl] cyclohexane (TAPC) (60 nm)/emitter X (20 nm)/ 2,2′2″-(1,3,5-benzinetriyl) tris(1-phenyl-1-*H*-benzimidazole) (TPBi) (35 nm)/LiF (1 nm)/Al (device I) were fabricated, whereas, MoO_3 works as the hole-injection layer; TAPC functions as the hole transporting layer; TPBi serves as the electron-transporting layer; and LiF acts as the electron-injection layer. The emitter "X" refers to TPP-Cz, TPP-2Cz, TPP-PhCz, and TPP-2PhCz, which act as the light-emitting layers for devices I-1, I-2, I-3, and I-4, respectively. As shown in **Table 3**, these devices except for device I-1 (TPP-Cz) exhibited bright deep-blue EL emission with the Commission Internationale de l'Elcairage (CIE) coordinates of (0.15, 0.11). Their turn-on voltages are ≈4.0 V with a maximum luminance (L_{max}) reached to ≈2000 cd m^{-2}, which is comparable to that of commercial OLED emitters. However, compared with the PL spectra of these AIEgens in film states, the EL ones exhibited obvious red-shifts and even 36 nm was observed in device I-1 (Figure S28, Supporting Information), implying the necessity for optimization of these devices.

Considering the favorable factors of valuable deep-blue OLEDs of these TPP-based AIEgens, such as the PL emission peak locations, FWHMs, emitting efficiencies in film states, AIE feature, and unique excited state characteristics as discussed above, TPP-Cz is a good candidate for the optimization of the device structures. Moreover, different functional layers were introduced to control the exciton recombination region to improve the device performance. The structures of newly designed devices II are shown in **Figure 8**.

First, the thickness of the hole (MoO_3) and electron (TPBi) transporting layers were adjusted to reduce the turn-on voltage, and the thick TAPC layer was replaced by a thin (4,4′,4″-tri(9-carbazoyl)triphenylamine) (TCTA) layer to block the electron transportation and fine-tune the exciton recombination region to the emitter layer because the red-shifted emission in device I-1 might originate from the interface between TPP-Cz and TAPC or TPBi. As expected, device II-1 not only exhibited a lower turn-on voltage but also produced unchanged emission profile compared with that of the PL spectrum, with λ_{max} located at 436 nm with CIE coordinates of (0.15, 0.10). In addition, the maximum current efficiency ($\eta_{C,max}$) (0.98 cd A^{-1}), external quantum efficiency ($\eta_{ext,max}$) (1.14%), and L_{max} (2433 cd m^{-2}) showed obvious improvement. However, its roll-off in η_C under high brightness ($\eta_{C,1000}$ = 0.58 cd A^{-1}, 40% off) is too severe.

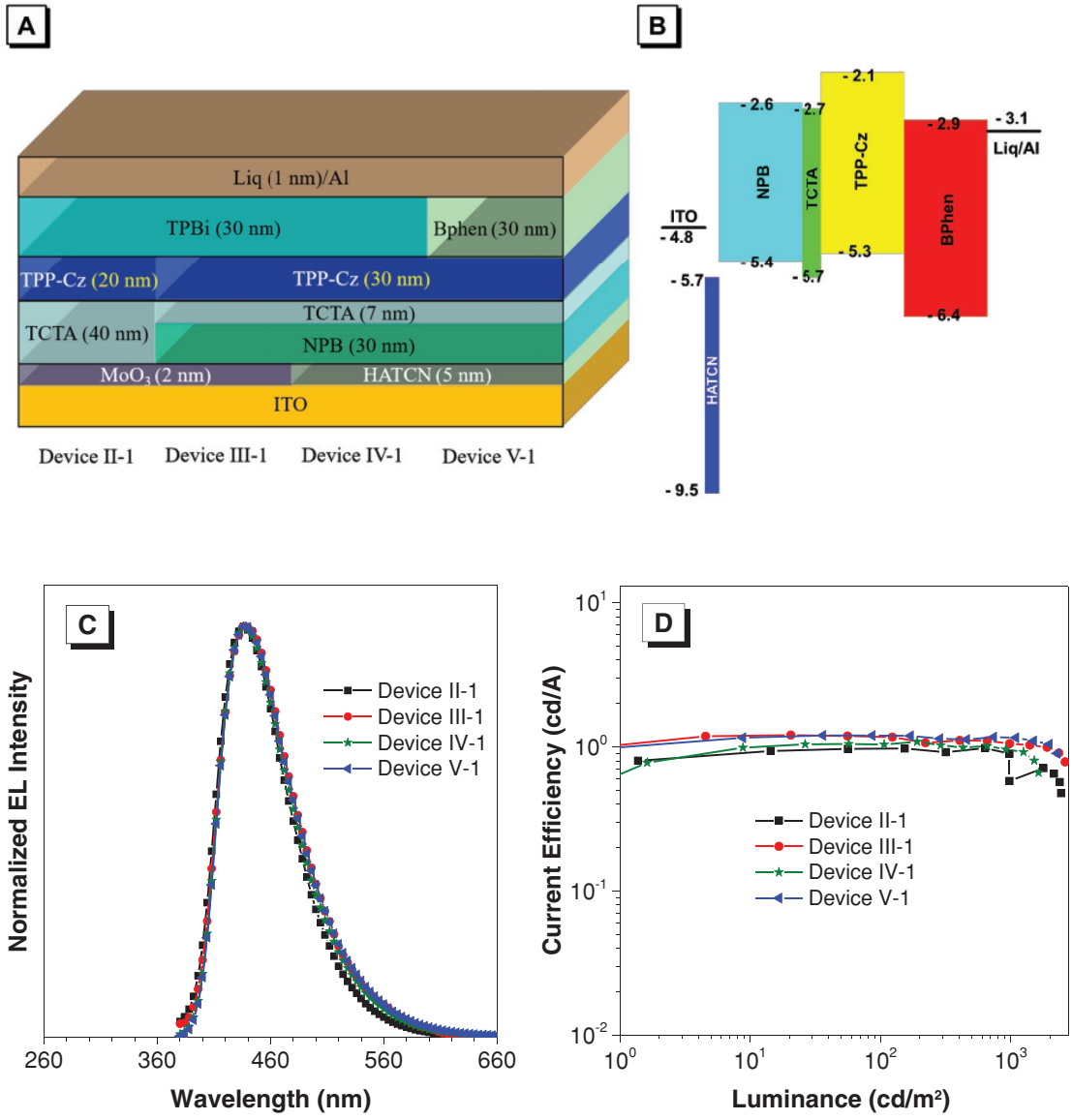

Figure 8. A) The configuration diagrams; B) the energy level and configuration of device V-1; C) EL spectra, and D) current efficiency–luminance characteristics of the devices II–1, III–1, IV–1, and V–1.

To increase the device stability, an *N*,*N*′-Bis(naphthalen-1-yl)-*N*,*N*′-bis(phenyl)benzidine (NPB) (30 nm) layer was added as a hole-modified layer, and the thin TCTA layer was retained as the electron barrier. Simultaneously, a thick emitter layer was introduced to ensure exciton recombination in the TPP-Cz layer, and similar deep-blue emission was exhibited in device III-1 with improved performance of $\eta_{C,max}$ (1.21 cd A^{-1}), $\eta_{ext,max}$ (1.25%), and L_{max} (2608 cd m^{-2}). Delightfully, the rapid roll-off in η_C under high brightness was blocked, and the value was decreased to 13% at L = 1000 cd m^{-2} in device III-1. Then, the inorganic hole-modified layer of MoO_3 was replaced by the organic hexaazatriphenylenehexacabonitrile (HATCN) to simplify the fabrication process in device IV-1. Although no change in the CIE coordinates was observed, the performance had clearly deteriorated, indicating that the exciton recombination situation was affected by the change of the hole-modified layer. Finally, a bathophenanthroline (Bphen) layer was employed to replace the TPBi as the electron-transporting/hole-blocking layer in device V-1, and improved performance with $\eta_{C,max}$ (1.20 cd A^{-1}), $\eta_{ext,max}$ (1.49%), and L_{max} (2264 cd m^{-2}) was achieved. The roll-off in η_C under the brightness of 1000 cd m^{-2} was less than 5%, indicating the excellent device stability. Thus, TPP is considered a very good AIE core with great potential for developing high-efficiency deep-blue emitters.

3. Conclusion

In this work, TPP-based deep-blue AIEgens of TPP-Cz and TPP-PhCz with a line-shaped structure and TPP-2Cz and TPP-2PhCz with an X-shaped pattern were designed and prepared. Systematic spectral analysis and theoretical calculations

demonstrated their unique photophysical behaviors. A tremendous enhancement of the radiative transition decay rate and a slight reduction of the nonradiative decay rate were observed when moving from the solution to solid and film states, which differed greatly from the behaviors of traditional AIEgens. Thanks to the special quinone conformation in excited states, X-shaped molecules exhibit nearly twice the fluorescence efficiency for the two luminescent axles compared with line-shaped structure in dilute solution, but two substituted groups provide more free volume for molecular motion and result in inferior luminescence in aggregate state. Owing to the valuable emission in their film states, the nondoped OLEDs with these TPP-based AIEgens as emitting layers exhibited good performance, whereas, the TPP-Cz-based device exhibited the optimal performance, with an external quantum efficiency of 1.49% and an ideal current efficiency roll-off of 3.3% at unchanged CIE coordinates of (0.16, 0.11). All these results indicate that TPP is very valuable and shows potential as a deep-blue AIE core for optoelectronic applications.

Supporting Information

Supporting Information is available from the Wiley Online Library or from the author.

Acknowledgements

L.P. and H.W. contributed equally to this work. This work was financially supported by National Natural Science Foundation of China (21788102, 51673118, and 51603127), Natural Science Fund of Guangdong Province (2016A030312002), the Innovation and Technology Commission of Hong Kong (ITC-CNERC14SC01), Science & Technology Program of Guangzhou (201804020027, 201804010218, and 201704030069), and the Fundamental Research Funds for the Central Universities (2017JQ013 and 2017B0036).

Conflict of Interest

The authors declare no conflict of interest.

Keywords

aggregation-induced emission (AIE), deep-blue emitters, organic light-emitting diodes, tetraphenylpyrazine (TPP), unique excited state

Received: December 1, 2018
Revised: December 20, 2018
Published online: January 7, 2019

[1] C. W. Tang, S. A. VanSlyke, *Appl. Phys. Lett.* **1987**, *51*, 913.
[2] H. Uoyama, K. Goushi, K. Shizu, H. Nomura, C. Adachi, *Nature* **2012**, *492*, 234.
[3] A. Tsuboyama, H. Iwawaki, M. Furugori, T. Mukaide, J. Kamatani, S. Igawa, T. Moriyama, S. Miura, T. Takiguchi, S. Okada, M. Hoshino, K. Ueno, *J. Am. Chem. Soc.* **2003**, *125*, 12971.
[4] L. S. Hung, C. H. Chen, *Mater. Sci. Eng. R* **2002**, *39*, 143.
[5] S. Kim, B. Kim, J. Lee, H. Shin a, Y. Park, J. Park, *Mater. Sci. Eng. R* **2016**, *99*, 1.
[6] A. P. Kulkarni, C. J. Tonzola, A. Babel, S. A. Jenekhe, *Chem. Mater.* **2004**, *16*, 4556.
[7] L. Chen, G. Lin, H. Peng, H. Nie, Z. Zhuang, P. Shen, S. Ding, D. Huang, R. Hu, S. Chen, F. Huang, A. Qin, Z. Zhao, B. Z. Tang, *J. Mater. Chem. C* **2016**, *4*, 5241.
[8] K. T. Ly, R. W. Chen-Cheng, H. W. Lin, Y. J. Shiau, S. H. Liu, P. T. Chou, C. S. Tsao, Y. C. Huang, Y. Chi, *Nat. Photonics* **2017**, *11*, 63.
[9] S. W. Thomas, G. D. Joly, T. M. Swager, *Chem. Rev.* **2007**, *107*, 1339.
[10] R. Jakubiak, C. J. Collison, W. C. Wan, L. J. Rothberg, B. R. Hsieh, *J. Phys. Chem. A* **1999**, *103*, 2394.
[11] S. A. Jenekhe, J. A. Osaheni, *Science* **1994**, *265*, 765.
[12] B. T. Nguyen, J. E. Gautrot, C. Ji, P. L. Brunner, M. T. Nguyen, X. X. Zhu, *Langmuir* **2006**, *22*, 4799.
[13] C. T. Chen, *Chem. Mater.* **2004**, *16*, 4389.
[14] J. Luo, Z. Xie, J. W. Y. Lam, L. Cheng, H. Chen, C. Qiu, H. S. Kwok, X. Zhan, Y. Liu, D. Zhu, B. Z. Tang, *Chem. Commun.* **2001**, 1740.
[15] Y. Hong, J. W. Y. Lam, B. Z. Tang, *Chem. Soc. Rev.* **2011**, *40*, 5361.
[16] J. Mei, N. L. C. Leung, R. T. K. Kwok, J. W. Y. Lam, B. Z. Tang, *Chem. Rev.* **2015**, *115*, 11718.
[17] P. Shen, Z. Zhuang, Z. Zhao, B. Z. Tang, *J. Mater. Chem. C* **2018**, *6*. 11835.
[18] J. Guo, Z. Zhao, B. Z. Tang, *Adv. Opt. Mater.* **2018**, *6*, 1800264.
[19] B. Chen, B. Liu, J. Zeng, H. Nie, Y. Xiong, J. Zou, H. Ning, Z. Wang, Z. Zhao, B. Z. Tang, *Adv. Funct. Mater.28*, **2018**, 1803369.
[20] Z. Ruan, L. Li, C. Wang, Y. Xie, Q. Hu, Q. Peng, S. Ye, Q. Li, Z. Li, *Small* **2016**, *12*, 6623.
[21] T. Liu, L. Zhu, C. Zhong, G. Xie, S. Gong, J. Fang, D. Ma, C. Yang, *Adv. Funct. Mater.* **2017**, *27*, 1606384.
[22] Y. Wang, Y. Liao, C. P. Cabry, D. Zhou, G. Xie, Z. Qu, D. W. Bruce, W. Zhu, *J. Mater. Chem. C* **2017**, *5*, 3999.
[23] A. Islam, D. Zhang, R. Peng, R. Yang, L. Hong, W. Song, Q. Wei, L. Duan, Z. Ge, *Chem. - Asian J.* **2017**, *12*, 2189.
[24] L. Yang, Y. Zhang, X. Zhang, N. Li, Y. Quan, Y. Cheng, *Chem. Commun.* **2018**, *54*, 9663.
[25] D. Lo, C. H. Chang, G. Krucaite, D. Volyniuk, J. V. Grazulevicius, S. Grigalevicius, *J. Mater. Chem. C* **2017**, *5*, 6054.
[26] S. Xiang, Z. Huang, S. Sun, X. Lv, L. Fan, S. Ye, H. Chen, R. Guo, L. Wang, *J. Mater. Chem. C* **2018**, *6*, 11436.
[27] L. Chen, Y. Jiang, H. Nie, P. Lu, H. H. Y. Sung, I. D. Williams, H. S. Kwok, F. Huang, A. Qin, Z. Zhao, B. Z. Tang, *Adv. Funct. Mater.* **2014**, *24*, 3621.
[28] X. Chen, Z. Yang, Z. Xie, J. Zhao, Z. Yang, Y. Zhang, M. P. Aldreda, Z. Chi, *Mater. Chem. Front.* **2018**, *2*, 1017.
[29] J. Li, R. Zhang, Z. Wang, B. Zhao, J. Xie, F. Zhang, H. Wang, K. Guo, *Adv. Opt. Mater.* **2018**, *6*, 1701256.
[30] H. Li, Z. Chi, X. Zhang, B. Xu, S. Liu, Y. Zhang, J. Xu, *Chem. Commun.* **2011**, *47*, 11273.
[31] N. Venkatramaiah, G. D. Kumar, Y. Chandrasekaran, R. Ganduri, S. Patil, *ACS Appl. Mater. Interfaces* **2018**, *10*, 3838.
[32] W. Qin, Z. Yang, Y. Jiang, J. W. Y. Lam, G. Liang, H. S. Kwok, B. Z. Tang, *Chem. Mater.* **2015**, *27*, 3892.
[33] J. J. Liang, Y. Li, Y. Yuan, S. H. Li, X. D. Zhu, S. Barlow, M. K. Fung, Z. Q. Jiang, S. R. Marder, L. S. Liao, *Mater. Chem. Front.* **2018**, *2*, 917.
[34] Y. Dong, J. W. Y. Lam, A. Qin, J. Liu, Z. Li, B. Z. Tang, *Appl. Phys. Lett.* **2007**, *91*, 011111.
[35] J. Chen, C. C. W. Law, J. W. Y. Lam, Y. Dong, S. M. F. Lo, I. D. Williams, D. Zhu, B. Z. Tang, *Chem. Mater.* **2003**, *15*, 1535.
[36] J. Yang, J. Huang, Q. Li, Z. Li, *J. Mater. Chem. C* **2016**, *4*, 2663.
[37] M. Chen, L. Li, H. Nie, J. Tong, L. Yan, B. Xu, J. Z. Sun, W. Tian, Z. Zhao, A. Qin, B. Z. Tang, *Chem. Sci.* **2015**, *6*, 1932.
[38] M. Chen, H. Nie, B. Song, L. Li, J. Z. Sun, A. Qin, B. Z. Tang, *J. Mater. Chem. C* **2016**, *4*, 2901.

[39] L. Pan, Y. Cai, H. Wu, F. Zhou, A. Qin, Z. Wang, B. Z. Tang, *Mater. Chem. Front.* **2018**, *2*, 1310.
[40] P. Karastatiris, J. A. Mikroyannidis, I. K. Spiliopoulos, A. P. Kulkarni, S. A. Jenekhe, *Macromolecules* **2004**, *37*, 7867.
[41] J. Mei, Y. Hong, J. W. Y. Lam, A. Qin, Y. Tang, B. Z. Tang, *Adv. Mater.* **2014**, *26*, 5429.
[42] H. Nie, K. Hu, Y. Cai, Q. Peng, Z. Zhao, R. Hu, J. Chen, S.-J. Su, A. Qin, B. Z. Tang, *Mater. Chem. Front.* **2017**, *1*, 1125.
[43] Y. C. Duan, Y. Wu, J. L. Jin, D. M. Gu, Y. Geng, M. Zhang, Z. M. Su, *ChemPhysChem* **2017**, *18*, 755.
[44] L. Wang, B. Xu, J. Zhang, Y. Dong, S. Wen, H. Zhang, W. Tian, *Phys. Chem. Chem. Phys.* **2013**, *15*, 2449.